Crystal structures, luminescent and thermal properties of a new series of lanthanide complexes with 4-ethylbenzoic acid†

Hong-Mei Ye, Ning Ren, Jian-Jun Zhang,* Shu-Jing Sun and Juan-Fen Wang

Received (in Victoria, Australia) 23rd September 2009, Accepted 26th October 2009
First published as an Advance Article on the web 25th January 2010
DOI: 10.1039/b9nj00504h

A series of lanthanide complexes with the 4-ethylbenzoic acid ligand (4-eba), $[Ln(4\text{-eba})_3(phen)]_2$ (Ln = Nd (**1**), Sm (**2**), Eu (**3**), Tb (**4**), Dy (**5**) and Ho (**6**); phen = 1,10-phenanthroline), have been synthesized and structurally characterized by single-crystal X-ray diffraction. In the isostructural complexes **1**–**4**, two Ln^{3+} ions are connected together by four bridging 4-eba ligands, with two of them in a bidentate-bridging mode and the other two in a bidentate chelating-bridging mode, and each Ln^{3+} is also chelated by one 4-eba group and one phen ligand, giving a coordination number of nine. In complex **5**, however, two eight-coordinated Dy^{3+} ions are held together only by two bidentate-bridging 4-eba ligands, and another two 4-eba ligands coordinate to one Dy^{3+} ion in a chelating mode. In complex **6**, each Ho^{3+} ion is eight-coordinated to four bidentate-bridging 4-eba ligands, one chelating 4-eba group and one chelating phen ligand. Thermal analysis of the six complexes is discussed by TG-DTG and IR techniques. The activation energy E values of the first decomposition stage for complexes **1**–**6** are calculated by integral isoconversional non-linear (NL-INT) and Ozawa iteration methods, respectively. The fluorescent properties of complexes **3** and **4** are also studied.

Introduction

Benzoic acid and some of its derivatives, which have been used as conservant, catalyst precursor polymers in pharmaceutical industries,[1] are always used as important organic ligands of lanthanide complexes. Recently, lanthanide complexes have aroused great attention not just because of their interesting and various structures, but also their applications in many fields, such as probes and sensors for natural and medical science,[2] liquid crystalline materials,[3] white LED devices[4] and so on.[5–7] Therefore, complexes about rare earth elements have been widely reported.[8–15] In this paper, we have synthesized a new series of complexes with the general formula of $[Ln(4\text{-eba})_3(phen)]_2$ [Ln = Nd (**1**), Sm(**2**), Eu (**3**), Tb (**4**), Dy (**5**) and Ho (**6**)]. Although each complex has the identical ligands, there are three different structures in the six complexes. Complexes **1**–**4** are isostructural. The structures of complex **5** and **6** are different from each other. It is noted that the structure of complex **5** is rare in lanthanide complexes because there are two bridging 4-eba groups and two 4-eba ligands which chelate one Dy^{3+} ion at the same time. In addition, the fluorescent and thermal properties of the six complexes are also studied.

Results and discussion

Infrared spectra

IR spectra data of the organic ligands and the complexes are listed in Table 1. The $\nu_{C=O}$ (–COOH) of the free ligand at 1685 cm^{-1} completely disappears in the IR spectrum of the complexes, whereas the characteristic peaks of $\nu_{as}(COO^-)$ and $\nu_s(COO^-)$ are observed at 1590–1557 and 1415–1424 cm^{-1}, respectively. These facts indicate that the oxygen atoms of the carboxylate groups are coordinated to the Ln^{3+} ion.[16] The band at 1646 cm^{-1}, which is assigned to the ν(C=N) stretch for the free phen ligand also shifts to lower wavenumber 1610–1603 cm^{-1} in complexes, suggesting that the nitrogen atoms of the phen ligand also coordinate to the Ln^{3+} ion. Meanwhile, the band at 410–419 cm^{-1} in the complexes assigned to ν(Ln–O) also demonstrates that the oxygen atoms of the carboxylate groups have formed a coordinative bond with Ln^{3+}.[17,18]

Table 1 Important IR bands of the ligands and complexes **1**–**6** (cm^{-1})

Compounds	$\nu_{C=N}$	$\nu_{C=O}$	$\nu_{as}(COO^-)$	$\nu_s(COO^-)$	ν(Ln–O)
Phen	1646	—	—	—	—
4-Heba	—	1685	—	—	—
$[Nd(4\text{-eba})_3(phen)]_2$	1603	—	1557	1415	416
$[Sm(4\text{-eba})_3(phen)]_2$	1609	—	1590	1416	418
$[Eu(4\text{-eba})_3(phen)]_2$	1609	—	1590	1416	412
$[Tb(4\text{-eba})_3(phen)]_2$	1610	—	1590	1417	417
$[Dy(4\text{-eba})_3(phen)]_2$	1610	—	1590	1417	419
$[Ho(4\text{-eba})_3(phen)]_2$	1610	—	1590	1424	410

Description of the crystal structures

Structures of the complexes 1–4. The structures of the complexes **1** and **2** are shown in Fig. 1 and Fig. 2, respectively. Selected bond lengths (Å) for the complexes **1**–**4** are listed in Table 2. Complex **1** is isostructural with the structures of complexes **2**, **3** and **4**; hence complex **1** is chosen as a representative. As shown in Fig. 1, the complex **1** has a crystallographic inversion center. Two Nd^{3+} atoms are

Experimental Center, Hebei Normal University, Shijiazhuang 050016, P. R. China. E-mail: jjzhang6@126.com; Fax: +86-31186268405; Tel: +86-31186269386

† CCDC reference numbers 711418, 711422, 728151–728153, 728155. For crystallographic data in CIF or other electronic format see DOI: 10.1039/b9nj00504h

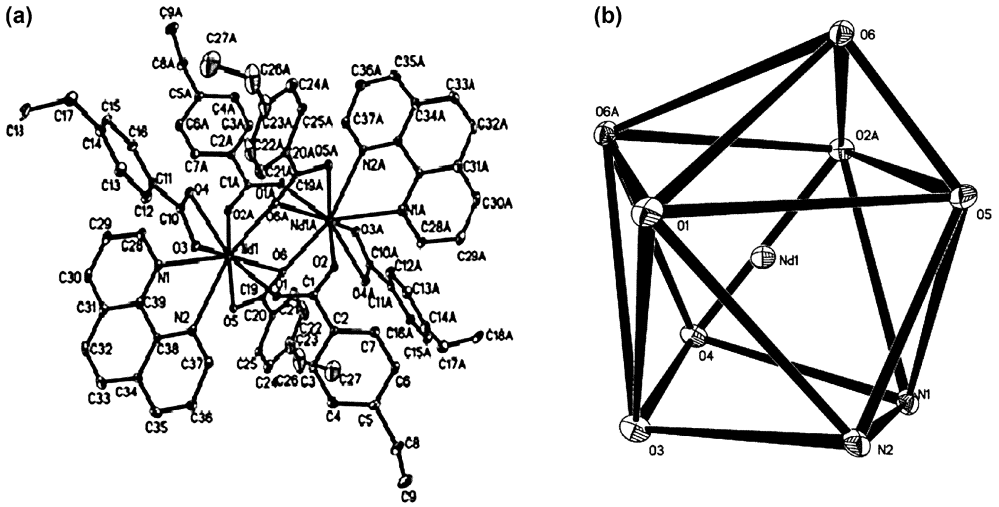

Fig. 1 (a) Molecular structure of complex **1** (A: $1-x, 1-y, 1-z$). All hydrogen atoms are omitted for clarity, and thermal ellipsoids are drawn at the 50% probability level. (b) Coordination geometry of the Nd^{3+} ion.

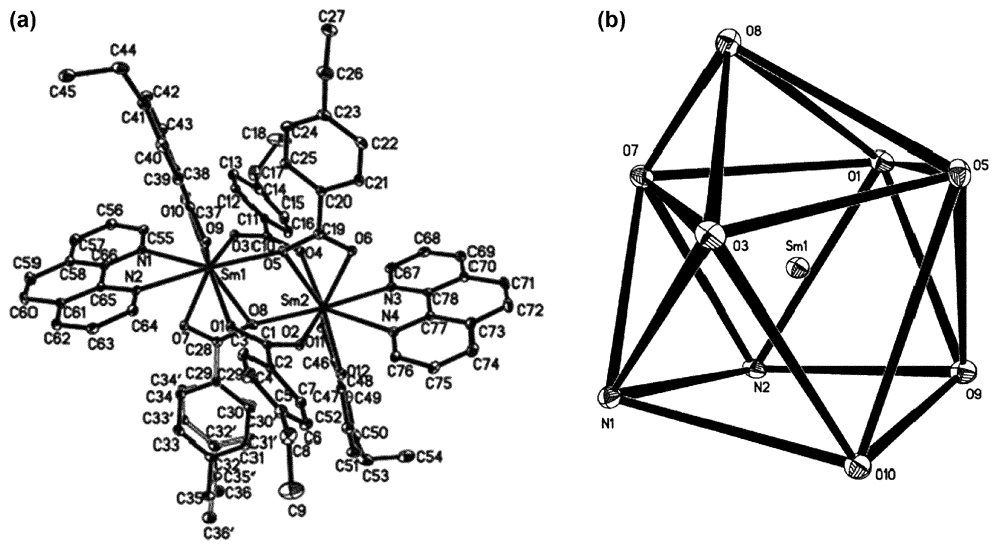

Fig. 2 (a) Molecular structure of complex **2**. All hydrogen atoms are omitted for clarity, and thermal ellipsoids are drawn at the 50% probability level. (b) Coordination geometry of the Sm^{3+} ion.

bridged together by four 4-eba groups, with two of them in a bidentate chelating-bridging mode, and the other two in a bidentate-bridging mode. In addition, each Nd^{3+} ion is further chelated by one 4-eba ligand and one phen molecule. The coordination number of the Nd^{3+} ion is nine and the distance between the two Nd^{3+} ions is 4.0196(5) Å. The coordination geometry of the Nd^{3+} ion is a distorted monocapped square-antiprism (Fig. 1b), with atoms O1, O5, O2A and O6A forming the upper and O3, O4, N1 and N2 forming the lower plane; atom O6 caps the upper plane. In addition, the structures of complexes **2**, **3** and **4** are isomorphous and there is no inversion center because of the disordered C29···C36 group.

The Nd–O bond lengths range from 2.412(2) to 2.7185(19) Å, with an average value of 2.565 Å. The Nd1–O6 bond (2.7185(19) Å) formed by the bidentate chelating-bridging carboxylates are the longest due to the instability of four-membered ring,[19] which can also be observed in other lanthanide carboxylate complexes. The average Nd–N distance is 2.658 Å. With respect to the complexes **2**–**4**, the average Ln–O bond distances are 2.461 Å for Sm, 2.4511 Å for Eu and 2.4291 Å for Tb, and the Ln–N distances are 2.629 Å for Sm, 2.617 Å for Eu and 2.594 Å for Tb. In the complexes **1**–**4**, the Ln–O and Ln–N bond lengths both become shorter upon going from Nd^{3+} to the Tb^{3+} ion, which may be explained by the lanthanide contraction.

Structure of complex 5. The crystal structure of complex **5** is shown in Fig. 3. Selected bond lengths (Å) for complex **5** are listed in Table 3. Complex **5** has a crystallographic inversion center. Each Dy^{3+} ion is coordinated by two oxygen atoms from two bridging 4-eba ligands, four oxygen atoms from two chelating 4-eba groups and two nitrogen atoms from one chelating phen molecule, giving a coordination number of eight. And Fig. 3b shows that the coordination polyhedron around Dy^{3+} is a trigondodecahedron. In the structure of

Table 2 Selected bond lengths (Å) for complexes **1**–**4**

Complex **1**					
Nd(1)–O(6)#1[a]	2.412(2)	Nd(1)–O(2)#1	2.413(2)	Nd(1)–O(1)	2.424(2)
Nd(1)–O(3)	2.462(2)	Nd(1)–O(5)	2.483(2)	Nd(1)–O(4)	2.495(2)
Nd(1)–N(1)	2.646(3)	Nd(1)–N(2)	2.670(3)	Nd(1)–O(6)	2.7185(19)
Nd(1)–Nd(1)#1	4.0196(5)				
Complex **2**					
Sm(1)–O(1)	2.3712(19)	Sm(1)–O(10)	2.423(2)	Sm(1)–N(2)	2.607(2)
Sm(1)–O(5)	2.3890(19)	Sm(1)–O(7)	2.446(2)	Sm(1)–N(1)	2.651(2)
Sm(1)–O(3)	2.3893(19)	Sm(1)–O(9)	2.482(2)	Sm(1)–O(8)	2.730(2)
Sm(1)–Sm(2)	3.9964(3)				
Complex **3**					
Eu(1)–O(1)	2.3608(18)	Eu(1)–O(10)	2.4113(18)	Eu(1)–N(2)	2.593(2)
Eu(1)–O(3)	2.3737(19)	Eu(1)–O(7)	2.4339(19)	Eu(1)–N(1)	2.641(2)
Eu(1)–O(5)	2.3778(18)	Eu(1)–O(9)	2.4754(19)	Eu(1)–O(8)	2.7248(19)
Eu(1)–Eu(2)	3.9921(3)				
Complex **4**					
Tb(1)–O(1)	2.337(2)	Tb(1)–O(10)	2.382(2)	Tb(1)–N(2)	2.571(3)
Tb(1)–O(5)	2.342(2)	Tb(1)–O(7)	2.401(2)	Tb(1)–N(1)	2.617(3)
Tb(1)–O(3)	2.343(2)	Tb(1)–O(9)	2.456(2)	Tb(1)–O(8)	2.743(2)
Tb(1)–Tb(2)	3.9814(4)				

[a] Symmetry transformations used to generate equivalent atoms: #1 $-x + 1, -y + 1, -z + 1$.

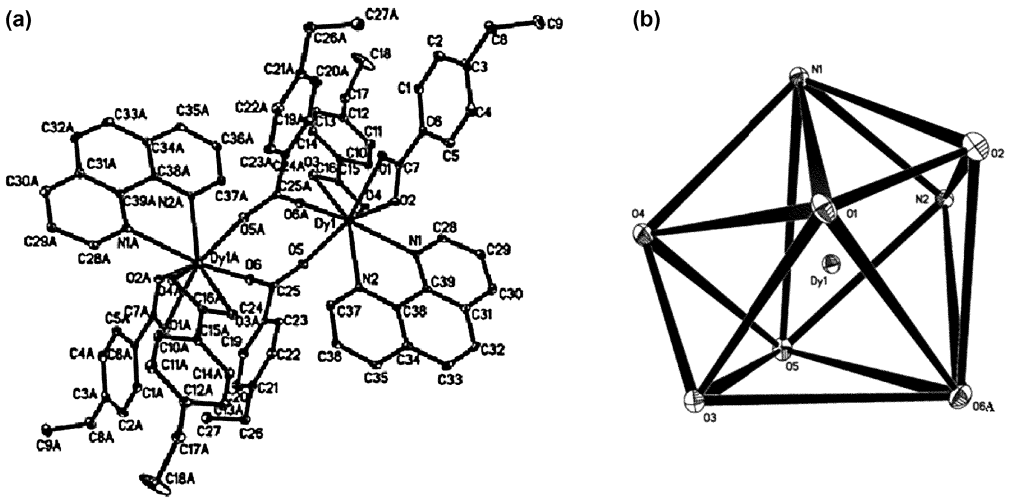

Fig. 3 (a) Molecular structure of complex **5** (A: $1 - x, 1 - y, 1 - z$). All hydrogen atoms are omitted for clarity, and thermal ellipsoids are drawn at the 50% probability level. (b) Coordination geometry of the Dy^{3+} ion.

Table 3 Selected bond lengths (Å) for complex **5**

Dy(1)–O(6)#1[a]	2.246(2)	Dy(1)–O(1)	2.377(2)	Dy(1)–N(1)	2.502(2)
Dy(1)–O(5)	2.325(2)	Dy(1)–O(2)	2.428(2)	Dy(1)–N(2)	2.519(2)
Dy(1)–O(4)	2.344(2)	Dy(1)–O(3)	2.453(2)		

[a] Symmetry transformations used to generate equivalent atoms: #1 $-x + 1, -y + 1, -z + 1$.

complex **5**, two Dy^{3+} ions are connected together only by two bridging carboxylate groups. And two carboxylate groups chelated one central Dy^{3+} ion at the same time. Such a structure is seldom reported and is interesting in lanthanide carboxylate complexes. The length of the Dy–O bonds is in the range of 2.246(2)–2.453(2) Å, with an average length of 2.36(7) Å. The mean bond distance of Dy–N is 2.511(8) Å.

Structure of complex 6. As shown in Fig. 4, complex **6** has an inversion center. The central Ho^{3+} ion is coordinated with four oxygen atoms from four bridging 4-eba groups, two oxygen atoms from one chelating bidentate 4-eba ligand and two nitrogens from one chelating phen ligand. Thus, the Ho^{3+} ion exhibits a coordination number of eight and the central Ho^{3+} ion has a distorted square-antiprism coordination geometry (Fig. 4b). One square face is formed by atoms N1, N2, O1, O2 and the other is formed by O3, O5, O4, O6A. Four 4-eba groups join two Ho^{3+} ions together in a bidentate-bridging mode, which is different from the former complexes **1**–**5**. Selected bond lengths (Å) for complex **6** are listed in Table 4. The average Ho1–O distance is 2.331 Å and the average Ho1–N distance is 2.556 Å.

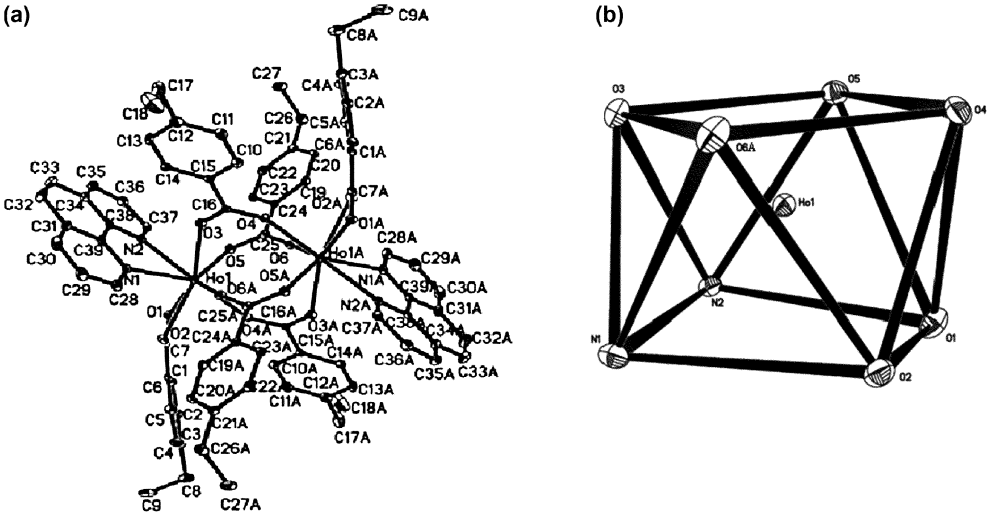

Fig. 4 Molecular structure of complex **6** (A: $1 - x$, $1 - y$, $1 - z$). All hydrogen atoms are omitted for clarity, and thermal ellipsoids are drawn at the 50% probability level. (a) Coordination geometry of the Ho^{3+} ion.

Table 4 Selected bond lengths (Å) for complex **6**

Ho(1)–O(6)#1[a]	2.271(2)	Ho(1)–O(5)	2.3271(19)	Ho(1)–N(2)	2.551(2)
Ho(1)–O(4)#1	2.291(2)	Ho(1)–O(2)	2.395(2)	Ho(1)–N(1)	2.560(2)
Ho(1)–O(3)	2.299(2)	Ho(1)–O(1)	2.404(2)		

[a] Symmetry transformations used to generate equivalent atoms: #1 $-x + 1$, $-y + 1$, $-z + 1$.

Fluorescence spectra

The excitation wavelengths of the complexes **3** and **4** in the solid state were performed in the range of 200–400 nm. The fluorescent spectra were observed in the range of 400–700 nm by selective excitation wavelength at 320 nm, as shown in Fig. 5 and Fig. 6. Complexes **3** and **4** exhibit red and green luminescence, respectively, under the radiation of UV light. For complex **3**, the emission peaks of the Eu^{3+} ion are observed at 579, 591 and 613 nm, corresponding to the $^5D_0 \rightarrow {}^7F_0$, $^5D_0 \rightarrow {}^7F_1$ and $^5D_0 \rightarrow {}^7F_2$ transitions, respectively. The intensity of the $^5D_0 \rightarrow {}^7F_2$ electric dipole transition is dependent on the degree of asymmetry in the environment of the Eu^{3+} ion, whereas the $^5D_0 \rightarrow {}^7F_1$ magnetic dipole transition is unrelated to the site asymmetry.

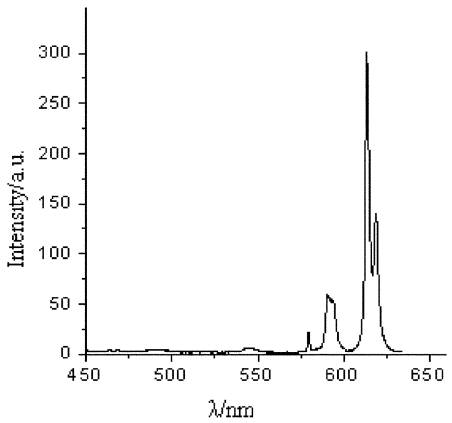

Fig. 5 Emission spectrum of complex **3** (λ_{ex} = 320 nm).

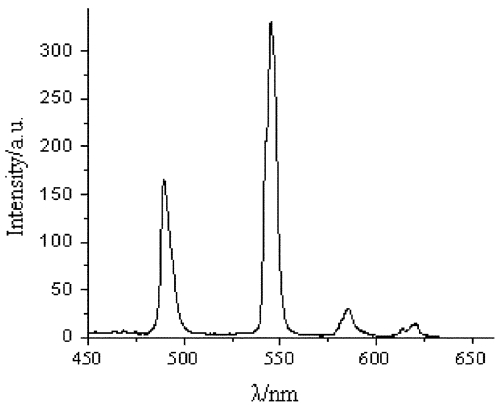

Fig. 6 Emission spectrum of complex **4** (λ_{ex} = 320 nm).

The intensity of the emitting band at 613 nm ($^5D_0 \rightarrow {}^7F_2$) is more intense than the others, indicating that there is no inversion center in the site of the Eu^{3+} ion.[20] For complex **4**, there are four main emission peaks in the luminescence spectra at about 490, 545, 585 and 619 nm, which are assigned to the $^5D_4 \rightarrow {}^7F_6$, $^5D_4 \rightarrow {}^7F_5$, $^5D_4 \rightarrow {}^7F_4$ and $^5D_4 \rightarrow {}^7F_3$ transitions of the Tb^{3+} ion, respectively. The strongest emission is at 545 nm due to the $^5D_4 \rightarrow {}^7F_5$ transition which is the preferred transition in terbium-containing complexes.[21]

Thermal analysis

The thermal analytical data for complexes **1**–**6** are listed in Table 5. The TG-DTG curves of complexes **1** and **4** recorded at 7 K min^{-1} are shown in Fig. 7 and Fig. 8, respectively. For complexes **2**, **3**, **5** and complex **6**, TG-DTG curves are similar

to complex **1** and complex **4**, respectively. Complexes **1** and **4** are chosen as a representative.

As shown in Fig. 7, there are two main successive mass loss stages. The first stage takes place from 482.31 K to 622.94 K, with a mass loss of 17.61% (calc. 23.34%), which corresponds to the loss of partial phen molecules. The second degradation occurs in the range of 622.94–907.75 K, in which the remaining phen molecules and 4-eba ligands are removed with a mass loss of 61.07%. Up to 907.75 K, the complex is completely degraded into Nd_2O_3 with a total mass loss of 78.68% (calc. 78.20%), which is confirmed by the similar characteristic absorption of the residue in IR spectra as the standard sample spectrum of Nd_2O_3. Complexes **2**, **3** and **5** all undergo the similar decomposition stages with complex **1**. Based on the above analysis, the thermal decomposition process of $[Ln(4\text{-eba})_3phen]_2$ [Ln = Nd(**1**), Sm(**2**), Eu(**3**) and Dy(**5**)] may be described as follows:

$$[Ln(4\text{-eba})_3phen]_2 \rightarrow [Ln_2(4\text{-eba})_6phen_{2-x}] \rightarrow Ln_2O_3$$

For complex **4**, as shown in Fig. 8, there are two mass loss stages. The first mass loss stage occurs at 475.60 K and ends at 648.45 K, with a mass loss of 23.22%, which coincides with the release of two phen molecules from the complex (calc. 22.91%). The second weight loss region occurs over the range of 648.45–887.47 K, where the ligands undergo the decomposition with a weight loss of 53.53% (calc. 53.33%). Up to 887.47 K, the TG-DTG curves do not change with the temperature, suggesting that a residue of Tb_4O_7 has been obtained, which is supported by the same characteristic absorption of the residue in IR spectra as the standard sample spectrum of Tb_4O_7. The thermal decomposition stage of the complex **6** is similar to complex **4**. So the thermal decomposition process of $[Ln(4\text{-eba})_3phen]_2$ (Ln = Tb(**4**) and Ho(**6**)) is predicted as follows:

$$[Tb(4\text{-eba})_3phen]_2 \rightarrow Tb_2(4\text{-eba})_6 \rightarrow 1/2Tb_4O_7$$

$$[Ho(4\text{-eba})_3phen]_2 \rightarrow Ho_2(4\text{-eba})_6 \rightarrow Ho_2O_3$$

Based on the analysis above, we can draw the conclusion that complexes **1**–**6** all have good thermostability until 470 K, which is related to the stable structures of the six complexes. Furthermore, Ln–N bonds of the complexes always break first in the thermal decomposition process, which can be explained by the longer Ln–N bond than that of the Ln–O bond.

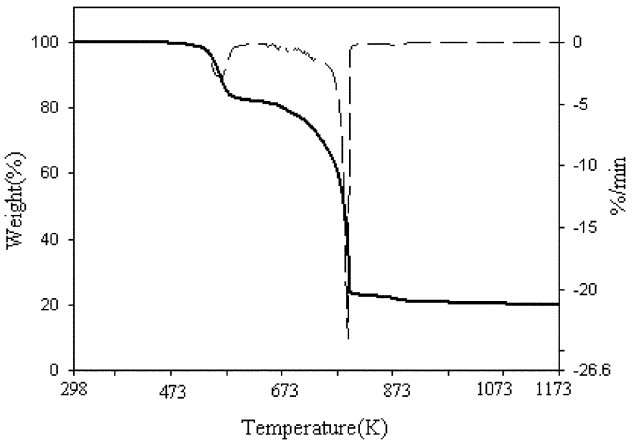

Fig. 7 TG-DTG curves of complex **1** at a heating rate of 7 K min^{-1}.

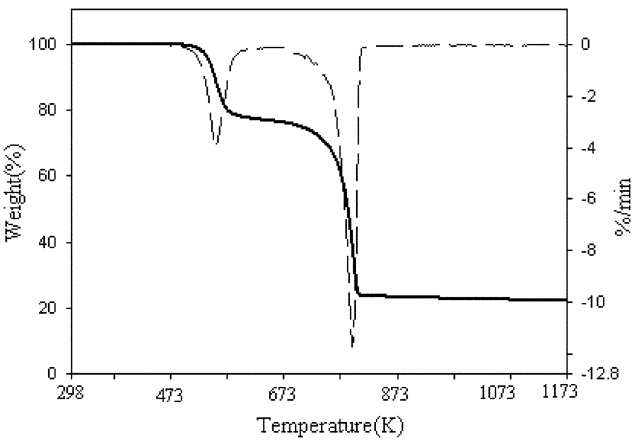

Fig. 8 TG-DTG curves of complex **4** at a heating rate of 7 K min^{-1}.

Kinetics of the first decomposition stage for complexes 1–6

The non-isothermal multiple scan method has been widely recognized in dealing with the thermal analysis data. The

Table 5 Thermal decomposition data for complexes **1**–**6** (β = 7 K min^{-1})

Complexes	Stage	Temperature range (K)	DTG peak temperature (K)	Mass loss rate/%		Probable removed groups	Residue
				Found	Calculated		
1	I	482.31–622.94	513.64	17.61	23.34[a]	*x* phen	$Nd_2(4\text{-eba})_6phen_{2-x}$
	II	622.94–907.75	794.63	61.07	54.86	6(4-eba) + (2 − *x*)phen − 3O	Nd_2O_3
2	I	487.72–641.77	560.12	19.70	23.16[a]	*x* phen	$Sm_2(4\text{-eba})_6phen_{2-x}$
	II	641.77–940.43	790.60	58.26	54.43	6(4-eba) + (2 − *x*)phen − 3O	Sm_2O_3
3	I	482.45–626.67	556.93	16.79	23.11[a]	*x* phen	$Eu_2(4\text{-eba})_6phen_{2-x}$
	II	626.67–980.12	773.25	60.93	54.32	6(4-eba) + (2 − *x*)phen − 3O	Eu_2O_3
4	I	475.60–648.45	552.41	23.22	22.91	2 phen	$Tb_2(4\text{-eba})_6$
	II	648.45–887.47	794.75	53.53	53.33	6(4-eba) − 3.5O	$1/2Tb_4O_7$
5	I	473.55–627.32	545.43	20.08	22.80[a]	*x* phen	$Dy_2(4\text{-eba})_6phen_{2-x}$
	II	627.32–927.45	788.34	57.18	53.59	6(4-eba) + (2 − *x*)phen − 3O	Dy_2O_3
6	I	475.44–613.56	560.94	23.02	22.73	2 phen	$Ho_2(4\text{-eba})_6$
	II	613.56–889.79	814.15	53.89	53.43	6(4-eba) − 3O	Ho_2O_3

[a] Theoretical value of the loss of 2phen.

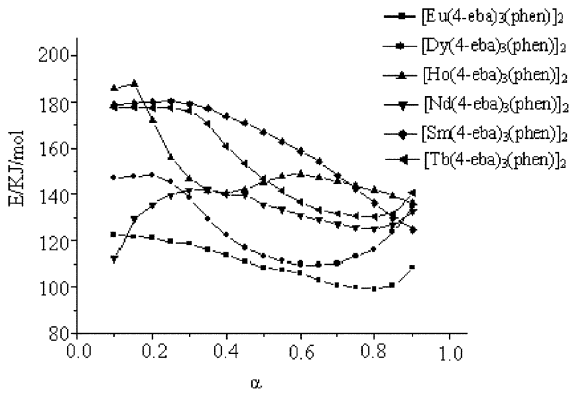

Fig. 9 The relationship between E and α by the NL-INT method.

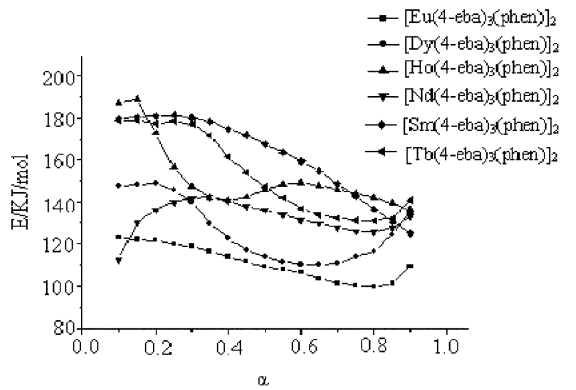

Fig. 10 The relationship between E and α by the Ozawa iteration method.

method does not involve the kinetic model function, thus the reliable value of the activation energy E can be obtained. Therefore, the intergral isoconversional non-linear (NL-INT)[22] and Ozawa iteration[23] methods are used to calculate the activation energy E of the first decomposition stage for complexes **1**–**6**. The relationship between E and α by the two methods is shown in Fig. 9 and Fig. 10, respectively. From Fig. 9 and Fig. 10, we can draw the conclusion as follows: the values of E corresponding to α which are calculated by the two methods are well consistent with each other, and the values of E accord with the general law (in the range of 80–50 kJ mol^{-1}).[24] The values of E about the six complexes vary with α obviously, indicating that the first decomposition stage is a multiple-step reaction.[25–27]

Conclusions

In summary, the crystal structures of a series of lanthanide complexes with the 4-eba ligand and phen involving three different structural types have been successfully obtained. Complexes **1**, **2**, **3** and **4** are isostructural. The Ln^{3+} ions have a typical coordination number of nine with a distorted mono-capped square-antiprism. The structure of complex **5** is very interesting in lanthanide complexes and the coordination geometry of Dy^{3+} is a trigondodecahedron. Complex **6** has a coordination number of eight and the coordination polyhedron of the Ho^{3+} ion is a distorted square-antiprism. The E values of the first decomposition stage for complexes **1**–**6** vary with α obviously, which indicates the complexity of the decomposition processes. In addition, complexes **3** and **4** exhibit the intense fluorescence properties.

Experimental

Materials and apparatus

Ln_2O_3, 4-ethylbenzoic acid and 1,10-phenanthroline were analytical reagents. $LnCl_3{\cdot}6H_2O$ was prepared by reaction of Ln_2O_3 and hydrochloric acid in aqueous solution.

Elemental analyses (C, H, N) were determined using an Elementar Vario-EL III analyzer, and the metal content was assayed using an EDTA titration method. IR spectra were measured on a Perkin-Elmer FTIR-1730 spectrometer in the range of 400–4000 cm^{-1} with KBr pellets. The molar conductance was determined on a Shanghai DDS-307 conductivity meter. The single-crystal X-ray diffraction data were obtained using a Saturn 724+ diffractometer. The fluorescent spectra were measured on an F-4500 Hitachi spectrophotometer in the solid state at room temperature. The TG-DTG experiments were carried out using a Perkin-Elmer TGA-7 thermogravimetric analyzer, and the heating rate was (3, 5, 7, 10 and 15) K min^{-1} for complexes **1**, **2**, **4**, **5** and **6** and (5, 7, 10 and 15) K min^{-1} for complex **3** from 298 to 1173 K with a static atmosphere.

Preparation of the complexes 1–6

$LnCl_3{\cdot}6H_2O$ (Ln = Nd (**1**), Sm (**2**), Eu (**3**), Tb (**4**), Dy (**5**) and Ho (**6**); 0.2 mmol) was dissolved in water. 4-Ethylbenzoic acid (0.6 mmol) and 1,10-phenanthroline (0.2 mmol) were dissolved in 95% C_2H_5OH solution. The pH value of the mixed ethanol solution was controlled within 5–7 with NaOH (1 mol L^{-1}) solution. Then the mixture of the two ligands was added dropwise into the $LnCl_3{\cdot}6H_2O$ solution, stirred for about 10 h at room temperature, and then deposited for 12 h. Subsequently, the precipitates were obtained by filtration and single crystals were collected from the mother liquor after three weeks at room temperature. Calc. for **1**: C, 60.68; H, 4.57; N, 3.63; Nd, 18.68%. Found: C, 60.63; H, 4.54; N, 3.71; Nd, 18.83%. Calc. for **2**: C, 60.23; H, 4.53; N, 3.60; Sm, 19.32%. Found: C, 59.85; H, 4.54; N, 3.60; Sm, 19.45%. Calc. for **3**: C, 60.08; H, 4.53; N, 3.59; Eu, 19.49%. Found: C, 59.48; H, 4.42; N, 3.78; Eu, 19.68%. Calc. for **4**: C, 59.55; H, 4.49; N, 3.56; Tb, 20.20%. Found: C, 59.20; H,4.53; N, 3.59; Tb, 20.17%. Calc. for **5**: C, 59.28; H, 4.46; N, 3.55; Dy, 20.56%. Found: C, 59.16; H, 4.47; N, 3.63; Dy, 20.88%. Calc. for **6**: C, 59.10; H, 4.46; N, 3.53; Ho, 20.81%. Found: C, 58.53; H, 4.46; N, 3.56; Ho, 21.03%.

Crystal structure determinations

The single-crystal X-ray data collection for complexes **1**–**6** was performed on a Saturn 724+ diffractometer with mono-chromated Mo-Kα radiation (λ = 0.71073 Å) at 293(2) K. All the structures were solved by direct methods using the program SHELXS-97 and refined by full-matrix least-squares methods on F^2 using the program SHELXL-97. The crystallo-graphic data and refinement parameters for the complexes

Table 6 Crystal data and structure refinement for complexes **1**–**6**

Parameter	Complex					
	1	**2**	**3**	**4**	**5**	**6**
Empirical formula	$C_{78}H_{70}N_4O_{12}Nd_2$	$C_{78}H_{70}N_4O_{12}Sm_2$	$C_{78}H_{70}N_4O_{12}Eu_2$	$C_{78}H_{70}N_4O_{12}$ Tb_2	$C_{78}H_{70}N_4O_{12}Dy_2$	$C_{78}H_{70}N_4O_{12}Ho_2$
M_r	1543.86	1556.08	1559.30	1573.22	1580.38	1585.24
Temperature (K)	293(2)	293(2)	293(2)	293(2)	293(2)	293(2)
Crystal system, space group	Triclinic, $P\bar{1}$	Triclinic, $P\bar{1}$	Triclinic, $P\bar{1}$	Triclinic, $P\bar{1}$	Monoclinic, $P2(1)/n$	Triclinic, $P\bar{1}$
a (Å)	10.8233(17)	12.1337(10)	12.1236(13)	12.0849(13)	10.0098(13)	10.5709(18)
b (Å)	12.664(2)	15.7800(14)	15.7615(18)	15.7273(18)	23.815(3)	11.734(2)
c (Å)	13.627(2)	18.7575(15)	18.7822(18)	18.7487(19)	13.7457(18)	13.976(3)
α (deg)	77.966(8)	77.814(2)	77.917(3)	77.978(3)	90	80.499(5)
β (deg)	79.457(8)	74.551(3)	74.750(3)	74.991(3)	93.593(2)	83.494(5)
γ (deg)	71.233(6)	87.505(3)	87.543(3)	87.569(3)	90	82.076(6)
Volume (A^3)	1716.1(5)	3383.4(5)	3385.6(6)	3366.1(6)	3270.3(7)	1686.1(5)
Z, $\rho_{calc.}$ (Mg m^{-3})	1, 1.494	2, 1.527	2, 1.530	2, 1.552	2, 1.605	1, 1.561
Absorption coefficient (mm^{-1})	1.562	1.786	1.903	2.151	2.337	2.397
$F(000)$	782	1572	1576	1584	1588	796
Crystal size (mm)	0.27 × 0.27 × 0.27	0.20 × 0.17 × 0.13	0.30 × 0.27 × 0.23	0.30 × 0.23 × 0.22	0.27 × 0.27 × 0.20	0.20 × 0.14 × 0.14
θ range (deg)	3.08–27.54	3.02–27.30	3.03–27.30	3.04–27.30	3.09–27.49	3.11–27.48
Limiting indices	$-12 \le h \le 1$, $-15 \le k \le 1$, $-17 \le l \le 15$	$-14 \le h \le 1$, $-17 \le k \le 2$, $-23 \le l \le 24$	$-15 \le h \le 1$, $-20 \le k \le 2$, $-24 \le l \le 21$	$-15 \le h \le 1$, $-20 \le k \le 2$, $-17 \le l \le 24$	$-12 \le h \le 1$, $-30 \le k \le 3$, $-17 \le l \le 17$	$-11 \le h \le 1$, $-15 \le k \le 1$, $-18 \le l \le 18$
Reflections collected/unique	14 111/7583 R_{int} = 0.0322	27 842/14 655 R_{int} = 0.0302	27 661/14 645 R_{int} = 0.0232	27 485/14 560 R_{int} = 0.0286	26 694/7385 R_{int} = 0.0321	13 930/7401 R_{int} = 0.0325
Completeness to θ = 27.49	95.7%	96.2%	96.1%	96.1%	98.5%	95.7%
Max. and min. transmission	0.6805 and 0.6805	0.7971 and 0.7165	0.6655 and 0.5991	0.6525 and 0.5646	0.6522 and 0.5742	0.7302 and 0.6457
Data/restraints/parameters	7583/0/436	14 655/19/894	14 645/19/900	14 560/19/900	7385/0/436	7401/0/436
Goodness of fit on F^2	1.005	1.000	0.999	1.001	0.999	1.003
Final R indices [$I > 2\sigma(I)$]	R_1 = 0.0359, wR_2 = 0.0725	R_1 = 0.0348, wR_2 = 0.0707	R_1 = 0.0313, wR_2 = 0.0699	R_1 = 0.0371, wR_2 = 0.0837	R_1 = 0.0302, wR_2 = 0.0676	R_1 = 0.0306, wR_2 = 0.0586
R indices (all data)	R_1 = 0.0405, wR_2 = 0.0750	R_1 = 0.0429, wR_2 = 0.0750	R_1 = 0.0389, wR_2 = 0.0747	R_1 = 0.0453, wR_2 = 0.0895	R_1 = 0.0337, wR_2 = 0.0699	R_1 = 0.0355, wR_2 = 0.0609
Largest diff. peak and hole (e $Å^{-3}$)	1.270 and −1.453	0.957 and −0.943	1.600 and −0.854	1.113 and −0.880	0.914 and −0.609	1.395 and −0.773

1–**6** are given in Table 6. In complexes **2**, **3** and **4**, 19 restraints were used in these three refinements. CCDC 728153, 728155, 728151, 728152, 711418 and 711422 contain the supplementary crystallographic data for complexes **1**, **2**, **3**, **4**, **5** and **6**.†

Acknowledgements

We thank the National Natural Science Foundation of China (No. 20773034) and the Natural Science Foundation of Hebei Province (No. B2007000237)

References

1 A. B. Siqueira, G. Bannach, E. C. Rodrigues, C. T. Carvalho and M. Ionashiro, *J. Therm. Anal. Calorim.*, 2008, **91**, 897–902.
2 Y.-L. Fu, J.-C. Zhang, Y.-G. Lv and W.-L. Cao, *Spectrochim. Acta, Part A*, 2008, **70**, 646–650.
3 M. Irfanullah and K. Iftikhar, *Inorg. Chem. Commun.*, 2009, **12**, 296–299.
4 C. Zheng, H.-J. Ren, Z.-F. Cui, F.-H. Chen and G.-Y. Hong, *J. Alloys Compd.*, 2009, **477**, 333–336.
5 Y.-M. Luo, J. Li, L.-X. Xiao, R.-R. Tang and X.-C. Tang, *Spectrochim. Acta, Part A*, 2009, **72**, 703–708.
6 K.-L. Wong, Y.-M. Zhu, Y.-Y. Yang, G.-L. Law, H.-H. Fan, P.-A. Tanner and W.-T. Wong, *Inorg. Chem. Commun.*, 2009, **12**, 1252–1254.
7 S. Dang, L.-N. Sun, S.-Y. Song, H.-J. Zhang, G.-L. Zheng, Y.-F. Bi, H.-D. Guo, Z.-Y. Guo and J. Feng, *Inorg. Chem. Commun.*, 2008, **11**, 531–534.
8 Y. Chen, Q. Chen, L. Song, H.-P. Li and F.-Z. Hou, *Microporous Mesoporous Mater.*, 2009, **122**, 7–12.
9 H.-X. Cui, J.-M. Chen, H.-D. Zhou and Y.-H. Lu, *Spectrochim. Acta, Part A*, 2007, **68**, 478–483.
10 C.-H. Yan, C.-F. Guo, P. Lu, M. Zhang and G.-M. Qiu, *J. Rare Earths*, 2007, **25**, 117.
11 Y. Huang, B. Yan and M.-J. Shao, *J. Solid State Chem.*, 2009, **182**, 657–668.
12 Y.-S. Song, B. Yan and L.-H. Weng, *Polyhedron*, 2007, **26**, 4591–4601.
13 A.-Q. Wu, F.-K. Zheng, W.-T. Chen, L.-Z. Cai, G.-C. Guo, J.-S. Huang, Z.-C. Dong and Y. Takano, *Inorg. Chem.*, 2004, **43**, 4839–4845.
14 Y. Li, F.-K. Zheng, X. Liu, W.-Q. Zou, G.-C. Guo, C.-Z. Lu and J.-S. Huang, *Inorg. Chem.*, 2006, **45**, 6308–6316.
15 J.-G. Kang, T.-J. Kim, H.-J. Kang, Y. Park and M.-K. Nah, *J. Lumin.*, 2008, **128**, 1867–1872.
16 Y.-Z. Shi, X.-Z. Sun and Y.-H. Jiang, *Spectra and Chemical Identification of Organic Compounds*, Science and Technology Press, Nanjing, 1988, p. 98.
17 C.-J. Xu, F. Xie, X.-Z. Guo and H. Yang, *Spectrochim. Acta, Part A*, 2005, **61**, 2005–2008.
18 R.-F. Wang, L.-P. Jin, M.-Z. Wang, S.-H. Huang and X.-T. Chen, *Acta Chim. Sin.*, 1995, **53**, 39–45.
19 A. W. H. Lam, W. T. Wong, S. Gao, G.-H. Wen and X.-X. Zhang, *Eur. J. Inorg. Chem.*, 2003, 149–163.
20 G.-D. Qian and M.-Q. Wang, *Mater. Res. Bull.*, 2001, **36**, 2289–2299.

21 M.-C. Yin, C.-C. Ai, L.-J. Yuan, C.-W. Wang and J.-T. Sun, *J. Mol. Struct*., 2004, **691**, 33–37.
22 S. Vyazovkin and D. L. Dollimore, *J. Chem. Inf. Comput. Sci*., 1996, **36**, 42–45.
23 Z. Gao, M. Nakada and I. Amasski, *Thermochim. Acta*, 2001, **369**, 137–142.
24 R.-Z. Hu, Z.-Q. Yang and Y.-J. Liang, *Thermochim. Acta*, 1988, **123**, 135.
25 S. Vyazovkin, *Int. Rev. Phys. Chem*., 2000, **19**, 45–60.
26 S. Vyazovkin and C. A. Wight, *Thermochim. Acta*, 1999, **53**, 340–341.
27 Z.-R. Lu, Y.-C. Ding, Y. Xu, S.-H. Chen and Y.-P. Yu, *J. Therm. Anal. Calorim*., 2003, **73**, 333–340.

